A novel adsorption differential volumetric apparatus to measure mass transfer in nanoporous materials

A Novel Adsorption Differential Volumetric Apparatus to Measure Mass Transfer in Nanoporous Materials

Jin-Yu Wang[a], Enzo Mangano[a], Stefano Brandani[a*], Federico Brandani[b] and Pluton Pullumbi[b]

[a] School of Engineering, The University of Edinburgh, King's Buildings, Edinburgh, EH9 3FB, UK

[b] Campus Innovation Paris, Air Liquide, Paris, France

Abstract

A novel adsorption differential volumetric apparatus was developed for the determination of diffusional time constants in nanoporous materials and applied to diffusion of nitrogen and argon in commercial pellets of 4A zeolite. The system is designed for high rates of data acquisition allowing to determine mass transfer time constants of seconds over the pressure range from vacuum to 130 kPa. Diffusion of N_2 and Ar on a single pellet and fragments obtained from the pellet are studied between –10 ℃ to 35 ℃ and 0.8 to 55 kPa. These systems are chosen as representing weak adsorption to demonstrate the sensitivity of the apparatus that gives a good signal-to-noise ratio even with a single pellet in the entire pressure range. The systems studied confirm micropore diffusion control and an isothermal diffusion model was shown to reproduce accurately the observed kinetics using reduced pressure plots. As the crystal size in the pellet is not known accurately, the resulting activation energies and the ratio of diffusional time constants of N_2 and Ar were used to validate the results against known literature values.

Keywords: Micropore diffusion; Argon and nitrogen; 4A zeolite; Adsorption kinetics; Volumetric apparatus.

1. Introduction

The knowledge of adsorption kinetics in commercial pellets is important for designing efficient gas separation processes. An accurate kinetic time constant can help to improve the process performance significantly [1]. Volumetric systems are widely used to measure mass transfer kinetics, but a recent review of common practices over the past 20 years [2] has highlighted the fact that in most cases these experiments are carried out with systems designed for equilibrium measurements. Typically large sample masses are used, which often lead to either bed effects [3] or heat effects [4, 5] and yield apparent diffusion time constants that can be several orders of magnitude lower than the true values [6].

The history of the use of the single branch volumetric apparatus for kinetic measurements can be dated back to the 1940s-1950s, where Barrer and co-workers investigated the potential of cation-exchanged zeolite for the kinetic separation of inert gases from atmospheric gases [7] and the temperature and concentration dependence of diffusivity for various gas-zeolite systems [8]. In the early 70s Riekert used a volumetric system to study the intracrystalline diffusion of ethylene in NiY zeolite [9] and the sorption rate controlling mechanism of hydrocarbons in zeolites used as catalysts [10]. In the following two decades, the volumetric technique was employed by several research groups for sorption kinetic studies [11–16]. In particular, Bülow and co-workers carried out extensive studies with the technique [17–26] covering also theoretical models; Hashimoto and co-workers used a volumetric system to measure intracrystalline diffusivities of hydrocarbons in HZSM-5, MFI- and Y-type zeolites [27–33]; the use of commercial volumetric systems for kinetic studies began to emerge from the 90s [34, 35]. From 2000 onwards there has been an increasing number of adsorption kinetic studies with both commercial and purpose-built volumetric systems, of which 90 cases have been summarised in the review [2]. It is worth mentioning that Farooq and co-workers [36–39] employed a single branch volumetric system that incorporates two differential pressure transducers (0 – 55.2 kPa full scale, FS) to study adsorption kinetics in carbon molecular sieves and silicates. A common reference cylinder was used to provide a constant reference pressure and its pressure differences with both dosing and uptake cells were measured [36–39].

A volumetric system designed for kinetic measurements should use small sample masses, typically below 50 mg; allow to change the configuration of the solid, including the addition of inert metal beads to increase the thermal mass of the system and ensure near isothermal conditions; use small pressure steps so that small changes in the adsorbed phase concentration can be monitored; and acquire data at a rate at least 10 times faster than the diffusional time constant being measured. Once the transient pressure data are collected, it is also important to use these directly in a reduced pressure plot [1] instead of converting the pressure data into uptake rate plots, introducing the assumption of negligible flow resistance between the dosing and uptake volumes, which can lead also to confusion as to which pressure is to be used at time zero [2]. A further key advantage of the use of the

reduced pressure plot is that it not only allows to determine unequivocally the time constant of the valve and that of the mass transfer process, but also identify which transport mechanism is dominating the response [1, 40].

The main challenge though is that for volumetric experiments the mass transfer information typically lies in the last 5% of the absolute pressure step. For example, if an adsorption step of 2 kPa at 50 kPa total pressure was to be performed with a pressure transducer with 100 kPa full scale, the mass transfer kinetics will be sensitive to the measurement of only 0.1% of the full scale and the signal-to-noise ratio will be too low to extract a reliable time constant. At low pressures the addition of a second low pressure transducer can be an improvement, but the need to maintain small pressure steps indicates that a better approach is the use of a differential pressure transducer in a two branch system, allowing to maintain essentially the same accuracy at the different pressure levels. In this regard, a differential volumetric system becomes the perfect candidate. It has an additional reference branch that contains no sample and symmetrical to the sample branch present in a conventional system. A differential pressure transducer is attached between the two branches to measure the adsorbed amount. Differential volumetric systems have been used mainly for high pressure hydrogen adsorption equilibrium studies [41–45]. It has been shown that the differential configuration significantly improves the accuracy of isotherm measurements and minimises the effect of temperature instability [42].

In this contribution we present a new Adsorption Differential Volumetric Apparatus (ADVA) designed for accurate determination of fast mass transfer kinetics in nanoporous materials from vacuum to atmospheric conditions. The main aim is to validate the new system through the study of N_2 and Ar diffusion in a single zeolite pellet of 4A and its fragments in the pressure range 0.8 to 55 kPa. These systems are chosen for their weak adsorption feature in order to demonstrate the high sensitivity of the ADVA. The N_2 – 4A system has been studied extensively [6, 46–53] while less data have been reported for Ar – 4A [50, 52–54], with both systems showing micropore diffusion control.

2. Theory

The model for a volumetric system [55] includes diffusion in the adsorbent and flow through the valve. The main assumptions are a linear isotherm; isothermal diffusion; and absence of external and bed resistances [55]. The form of response curves and the limiting cases have been demonstrated in detail [1, 2, 40, 55]. The analysis is based on the reduced pressure in the sample dosing cell [1, 2]

$$\sigma_D(\mathrm{t}) = \frac{P_{ds}(\mathrm{t}) - P_s^{\infty}}{P_{ds}^{0} - P_s^{\infty}} = \sum_{n=1}^{\infty} a_n \exp\left(-\beta_n^2 \frac{D}{R_P^2} t\right) \qquad (1)$$

with the dimensionless parameters

$$\gamma = \frac{1}{3R_gT_{us}}\frac{(P_s^\infty - P_{us}^0)V_{us}}{(q_\infty - q_0)V_S};\ \delta = \frac{1}{3R_gT_{ds}}\frac{(P_s^\infty - P_{us}^0)V_{ds}}{(q_\infty - q_0)V_S};\ \omega = \frac{R_gT_{ds}}{V_{ds}}\frac{\bar{\chi}R^2}{D} \tag{2}$$

$$\beta_n \cot\beta_n - z_n = 0;\ z_n = 1 + \gamma\beta_n^2 + \frac{\omega\delta\beta_n^2}{\omega - \beta_n^2} \tag{3}$$

and

$$a_n = \frac{1 + 3\delta + 3\gamma}{1 + 3\gamma}\frac{2\omega^2\delta\beta_n^2}{2\omega^2\delta\beta_n^2 + (\omega - \beta_n^2)^2(\beta_n^2 + z_n^2 - z_n + 2\gamma\beta_n^2)} \tag{4}$$

There will be a root to Eq. 3 in each π interval and an additional root in the interval where $\omega = \beta_n^2$ occurs. It is usually sufficient to sum the roots in the first 200 π intervals and check that the additional root is included in the calculated range.

The parameters δ and γ represent 1/3 of the ratio of the accumulation in the gas phase and adsorbed phase for the dosing and uptake cells, respectively. These are not regressed but determined directly from the initial and final pressures of the system as the overall mass balance of the system gives

$$(q_\infty - q_0)V_S = \frac{(P_{us}^0 - P_s^\infty)V_{us}}{R_gT_{us}} + \frac{(P_{ds}^0 - P_s^\infty)V_{ds}}{R_gT_{ds}} \tag{5}$$

The parameter ω is the ratio of the diffusion time constant to valve time constant. If the diffusional resistance is much greater than the valve resistance ($\omega > 4\pi^2$), the pressure response curve clearly shows two slopes, a short time slope limited by the valve and a long time decay limited by mass transfer inside the adsorbent. The two parameters, the diffusion time constant $\frac{R^2}{D}$ and ω, are obtained from the slopes of the experimental long-time and short-time exponential decays, respectively [1]. A deviation in the long-time asymptote intercept between the model and experimental data may indicate the presence of secondary effects such as non-linearity, heat effects or surface barrier resistance, as these effects will lead to a shift of the intercept [2].

The absolute mode and differential mode experiments in an ADVA are depicted in Fig. 1. For absolute mode experiments the pressure in the reference branch is equal to the initial dosing pressure P_{ds}^0. The reduced differential pressure is essentially the same as the reduced absolute pressure from traditional single-branch volumetric experiments and the same model can be applied

$$\sigma_{ds}(\mathrm{t}) = \sigma_D(t) = \frac{P_{ds}(\mathrm{t}) - P_s^\infty}{P_{ds}^0 - P_s^\infty} = \frac{(P_{ds}(\mathrm{t}) - P_{ds}^0) - (P_\infty - P_{ds}^0)}{(P_{ds}^0 - P_{ds}^0) - (P_s^\infty - P_{ds}^0)} = \frac{\Delta P(\mathrm{t}) - \Delta P^\infty}{\Delta P^0 - \Delta P^\infty}. \tag{6}$$

For differential mode experiments, the reduced differential pressure is not equivalent to the reduced pressure $\sigma_D(\mathrm{t})$ due to the varying reference pressure. The model needs to be modified to take into account the reference response which is essentially controlled by the valve resistance

$$\sigma_{dr}(t) = \frac{P_{dr}(\mathrm{t}) - P_r^{\infty}}{P_{dr}^0 - P_r^{\infty}} = \exp\left(-\frac{P_{dr}^0 - P_{ur}^0}{P_{dr}^0 - P_r^{\infty}}\omega_r t\right), \tag{7}$$

where ω_r is the ratio of diffusional time constant to the valve constant in the reference branch. For strongly adsorbed systems, the flow through the valve in the reference branch will be considerably smaller than the sample branch. Therefore ω_r should be smaller than ω [2] and it may be necessary to determine ω_r separately by performing an expansion in the reference branch only. For the weakly adsorbed systems under study here, ω_r is assumed to be equal to ω which is determined from the absolute mode experiments.

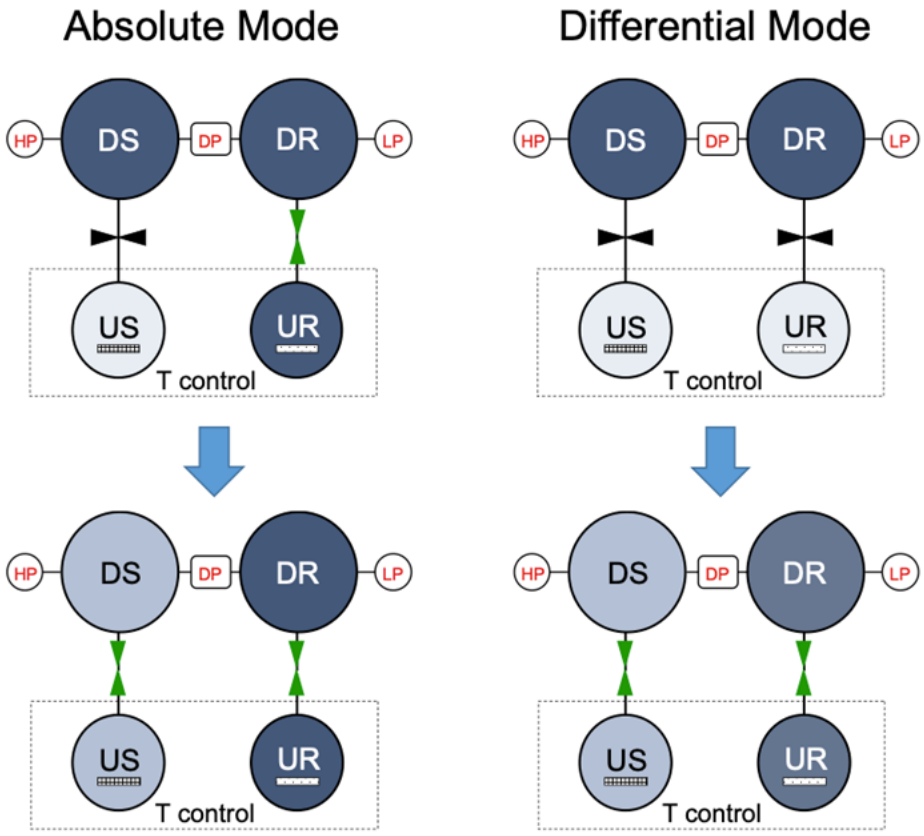

Fig. 1. Two ways of operating an ADVA: absolute mode and differential mode experiments. D stands for dosing; U for uptake; S for sample side; and R for reference side. In the US cell the adsorbent sample is mixed with inert metal beads while in UR only metal beads with a similar volume are loaded. Colour is an indication of the absolute pressure.

The reduced differential pressure in differential mode is

$$\sigma_D^{diff} = \frac{\sigma_{ds}(\mathrm{t})(P_{ds}^0 - P_s^\infty) - \sigma_{dr}(t)(P_{dr}^0 - P_r^\infty)}{\Delta P^0 - \Delta P^\infty}. \quad (8)$$

In a real experiment, there is always a time difference between the opening of the valves in the different branches. It is possible to apply a time lag to the reference response and it becomes $\sigma_{dr}(t - \Delta t)$. On the ADVA-1, this time difference Δt is around 0.01s and its effect on the determination of R^2/D was found to be negligible.

3. Experimental

ADVA-1 (adsorption differential volumetric apparatus – 1 bar)

The ADVA-1, a differential volumetric apparatus, was designed and purposely built in our laboratory for fast adsorption kinetic measurements from vacuum to near ambient pressures. The schematic diagram is shown in Fig. 2. The system consists of gas inlet lines, the core differential volumetric part, vent and vacuum lines.

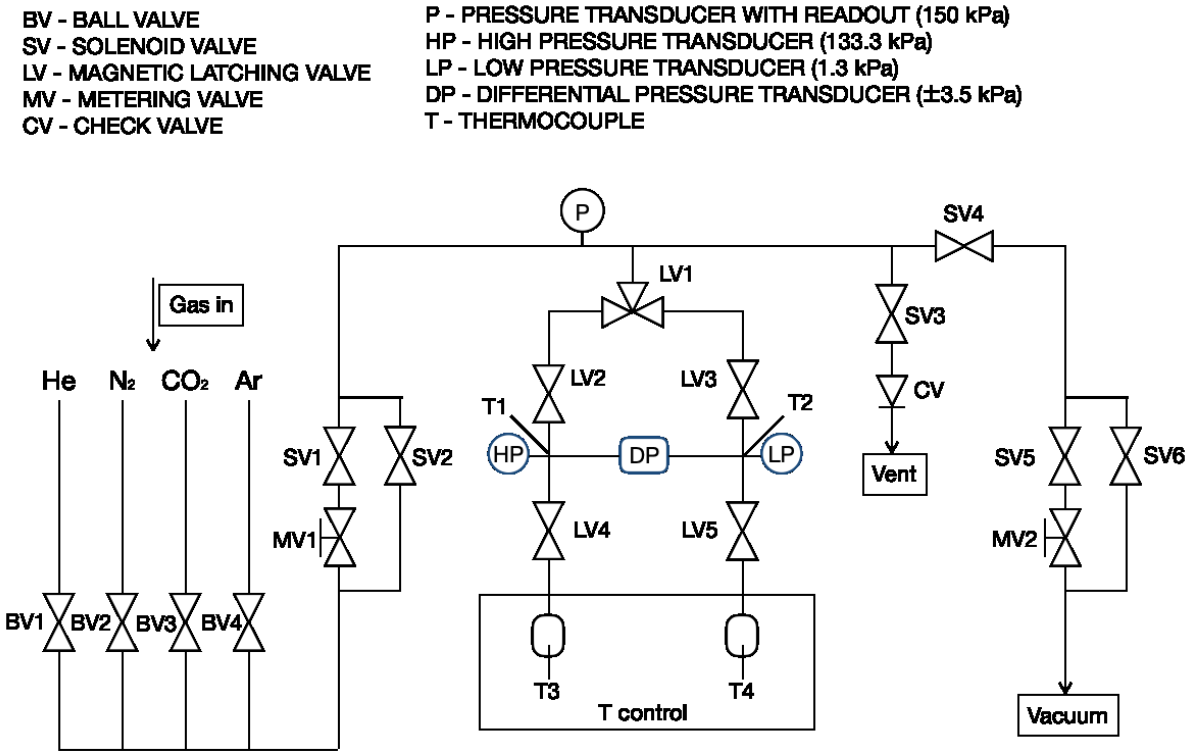

Fig. 2. Schematic diagram of the ADVA-1

The core differential part is made up of Swagelok® VCR parts and welded parts (Fig. 3). There are two symmetrical branches, a sample branch and a reference branch. Each branch is composed of a dosing volume and an uptake volume. A GE Druck PMP5028 differential pressure transducer with ±3.5 kPa full scale is attached between the two dosing volumes. It has an accuracy of ±0.04% FS BSL which takes into account the effect of non-linearity, hysteresis and repeatability. Two MKS 626C pressure transducers (accuracy 0.25% of reading) are used to monitor the absolute pressures in the system. A 133.3 kPa FS transducer is attached on the sample dosing cell whereas a 1.3 kPa transducer is attached on the reference side. Along with the differential transducer, the pressures of two dosing cells can be accurately measured at both low pressure and high pressure. On the uptake side, the sample and inert material (reference) holders are adapted from Swagelok® VCR ½ inch blind glands. The gland is drilled to create an internal volume and at the bottom a 1/16 inch tube fitting is welded to insert a thermocouple. K type reduced tip fast response thermocouples (Omega TJFT72, 1/16 inch diameter) are inserted into the sample and reference holders as well as the two dosing cells (see Fig. 3).

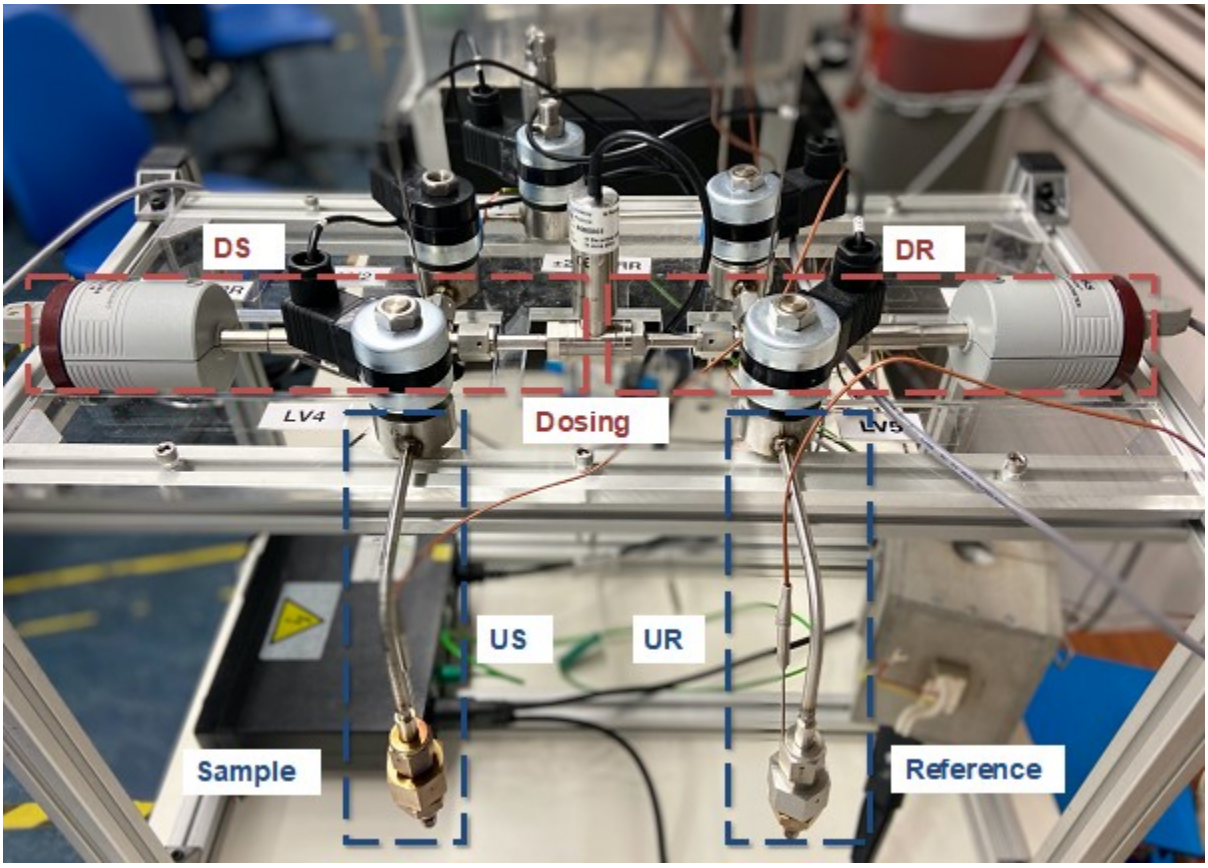

Fig. 3. Core differential volumetric part (DS: sample dosing, US: sample uptake, DR: reference dosing, UR: reference uptake).

Magnetic latching valves are used in the core part. The actuation of the valves is realised by moving the internal plunger with magnetic forces provided by solenoid coils and permanent magnets. There are two main advantages. Firstly, the valves only require a short pulse of

power input to latch or unlatch. The plunger can then be held in the latched position by the sole force of the permanent magnet or remain in the unlatched position. This means no continuous electrical power is required to hold the valve in either position, thus avoiding generating heat and changing the temperature profile of the system. The other advantage is that the internal volume of the valve stays the same for both positions. This is especially important for systems with small volumes and hence high sensitivity. A small valve internal volume change can have non-negligible impact on the mass balance.

To calibrate the cell volumes, stainless steel beads with known volume are used. By performing He expansion experiments with empty uptake cells and the cells filled with beads, the volume ratios between dosing and uptake are obtained and the cell volumes are calculated (Table 1). The cell volumes are very small compared to most of the volumetric systems present in literature [36, 56–62]. This is to increase the sensitivity of the system and to allow to reduce the amount of sample in the kinetic tests.

Table 1. ADVA core part cell volumes

	Sample branch $\times 10^6$	Reference branch $\times 10^6$
Dosing volume V_d , m^3	15.193	15.665
Uptake volume V_u , m^3	8.432	8.522

The sample regeneration is performed in-situ. This is realised by setting up the system configuration with the sample and reference holders in a vertical orientation while the rest of the core is on a horizontal plane (Fig. 3). As the sample holder is enclosed and heated by an oven, all the parts on the horizontal plane, especially the most vulnerable LV4, are away from the heat. T3, the thermocouple that measures the temperature inside the sample uptake cell, is connected to a Eurotherm 3216 process controller during sample regeneration. The controller has an 8 segment setpoint programmer that allows the desired temperature ramping and dwelling process to be set up. As over-temperature protection, an additional thermocouple is inserted into the oven and connected to a Tempatron on/off mode temperature controller (TC4810-02, 0 to 400℃). On the on/off controller the maximum temperature is set at around 395 ℃. In-situ regeneration greatly simplifies the kinetic testing procedure and avoids the possible air contamination of sample during transfer if the regeneration is performed on a separate station. Once the sample is loaded, all the relevant parameters for kinetic analysis can be measured without opening the cell.

As shown in Fig. 2, a part of the sample and reference uptake cells are controlled at the process temperature. For a differential volumetric system it is crucial to maintain symmetry on the two sides, which includes a symmetric temperature profile. For this reason, a bath with a weir is used to ensure that the circulating liquid covers the two branches in the same

way. The fluid temperature and circulation are controlled by a thermostatic circulating bath (Thermofisher Haake SC100).

The data acquisition and the operation of solenoid and magnetic latching valves are controlled by a Labview program. Pressure signals from HPT, LPT and DPT are acquired at 100 Hz while the temperature signal is acquired at 10 Hz which is limited by the thermocouple response time.

Zeolite 4A Sample

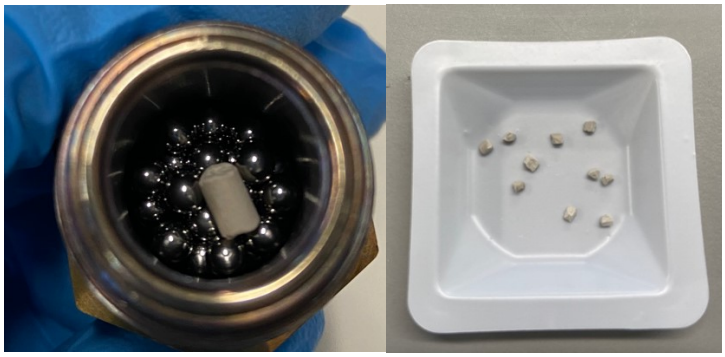

Fig. 4. The two samples used for the kinetic study. Left: A single pellet of zeolite 4A (41mg) loaded in the sample holder. Right: 10 fragments cut from pellets (46mg).

In this study, a single pellet of UOP zeolite 4A (Lot No. 2102004052, base diameter ~3.1mm and length ~5.2mm) and 10 fragments (~1.7×1.7×1.7 mm) cut from pellets (Fig. 4) have been used. The weight of the wet sample is 41mg for the pellet and 46 mg for the fragments. The crystal size of the sample is not known accurately.

In order to achieve isothermal conditions, the 4A sample and 120 stainless steel beads of 1/8'' diameter are mixed and loaded into the sample holder. The use of the stainless steel beads results in increased thermal mass as well as increased heat transfer surface area for the sample. It also offers an additional advantage of reducing the void uptake volume and accordingly increasing the sensitivity of the analysis.

The sample is degassed in-situ under vacuum with a turbomolecular pump (Pfeiffer HiCube 80 Eco). The regeneration of the sample is achieved by heating the cell at a ramping rate of 1℃/min up to 110℃. The temperature is held at 110℃ for 2 hours, followed by a further ramping rate of 1℃/min up to 350℃. The temperature is held at 350℃ for 6 hours, after which it is cooled to start the experiment.

Void volume and temperature zone calibration

After the regeneration, He expansion experiments were performed at room temperature first to determine the void cell volume. Next the bath was raised to submerge the sample and reference holders. Once thermal equilibrium was reached, the expansion experiments

were repeated. This was used to determine the fraction of the uptake volume at the bath temperature.

Diffusion measurements

As shown in Fig. 1, for the differential mode experiments, expansion happens in the two branches simultaneously and the initial uptake and dosing pressures for the two are the same. To start an experiment, the whole system is brought to the initial uptake pressure P_{us}^0. LV4 and LV5 are closed to isolate the uptake cells and the dosing cells are then charged to the target dosing pressure P_{ds}^0. LV1, LV2 and LV3 are closed to isolate the two sides, after which the adsorption is initiated by opening LV4 and LV5 and the pressure response is acquired until equilibrium is reached. The desorption experiment at the same pressure level is performed directly after to check for isotherm linearity over the step [2]. The final equilibrium pressure of the adsorption step becomes the initial uptake pressure for the desorption step. The desorption pressure step is similar to the adsorption.

For the absolute mode experiments, LV5 is kept open throughout and the expansion only happens in the sample branch. The conditions investigated first are small pressure steps (e.g. $P_{ds}^0 - P_{us}^0$ <2.5 kPa) where the segment of the isotherm is close to linear. Experiments were carried out at 5℃, 20℃ and 35℃ and the pressure range of 0.8 to 55 kPa.

4. Results and discussion

In this section we present the first experimental results from the ADVA-1 with the aim of validating the new apparatus and the technique. N_2 and Ar diffusivities in zeolite 4A single pellet and fragments are determined and compared to literature values.

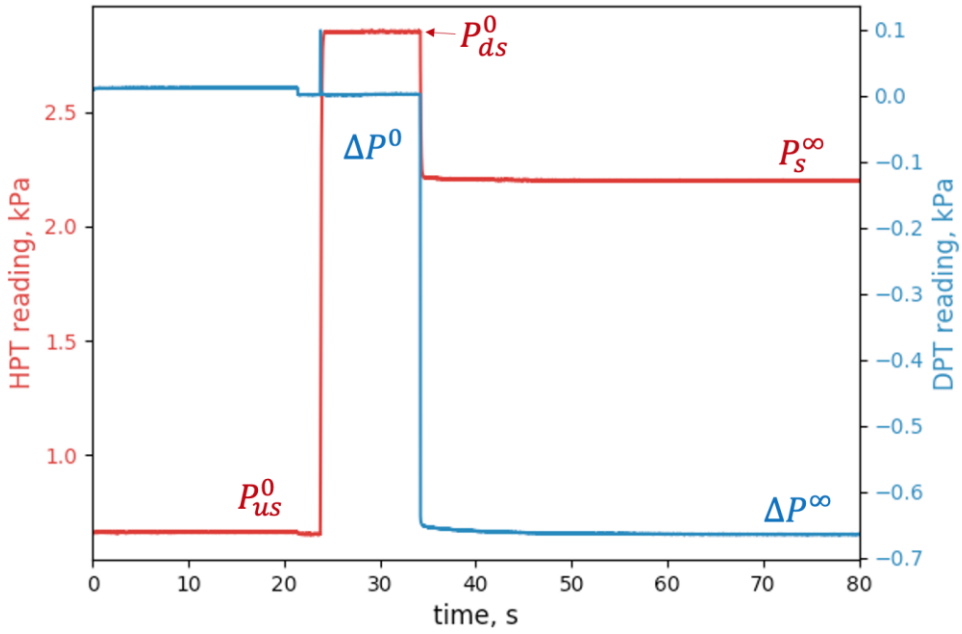

Fig. 5. Raw signal from HPT and DPT during a typical absolute mode experiment (N_2 on 4A single pellet at 35℃).

Fig. 5 shows raw HPT and DPT signals during a typical adsorption kinetic experiment (absolute mode). The whole experiment lasts less than 100s. The HPT signal clearly indicates the dosing step after isolating the sample uptake cell while the adsorption starting time is obvious from both HPT and DPT signals. The equilibrium pressures P_{us}^{0}, P_{ds}^{0} and P_{s}^{∞} are extracted from the HPT signal and they are used to calculate the adsorbed amount. ΔP^{0} and ΔP^{∞} are extracted from the DPT signal and used for the conversion to the reduced differential pressure.

Experimental checks for isothermality and linearity

Before using the volumetric model to match adsorption kinetic data from the experiments, the validity of the underlying assumptions of the model needs to be checked:

1. The process is isothermal.
2. The isotherm over the pressure step is linear.
3. There are no external or bed mass transfer resistances.

As discussed before, experiments have been performed with the aim of minimising heat effects by using a small mass of sample and inserting stainless steel beads. Pressure steps were kept small for isotherm linearity while checking that a satisfactory signal was obtained. To check the validity of the assumptions the recommendations given in [2] for the workflow of experiments were followed.

First, examine assumptions 1 and 3 by comparing the kinetics of pellet and fragment runs, i.e. changing sample configuration. As evident from the reduced pressure plot (Fig. 6), the consistency between the N_2 adsorption kinetics on the two samples at similar conditions confirmed that the system was indeed isothermal and external/bed resistances were negligible. The same conclusion was found for the Ar-4A system and the comparison of pellet and fragment results is reported in the Supplementary Information. The fact that the adsorption kinetics were independent of the sample particle size confirms that the system was under micropore diffusion control, in agreement with previous findings [46, 49].

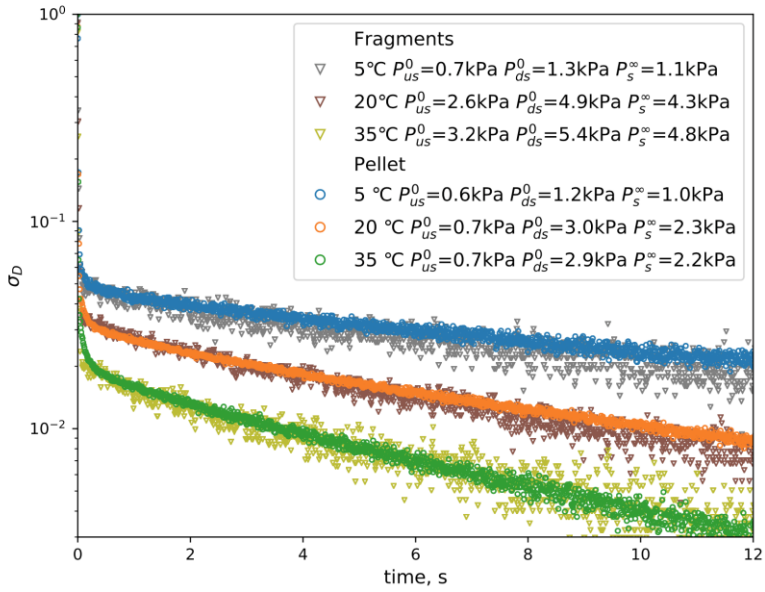

Fig. 6. Comparison of N_2 adsorption dynamics on 4A fragments and a single pellet at 3 temperatures.

In order to check assumption 2, a desorption experiment with the same step size was performed along with each adsorption experiment. It was found that adsorption and desorption curves overlap at all conditions, thus confirming isotherm linearity over the steps. An example of adsorption-desorption kinetics comparison is reported in the Supplementary Information. Having established the validity of the three assumptions, the isothermal volumetric model was applied to the experiment data.

Comparison of HPT and DPT signals

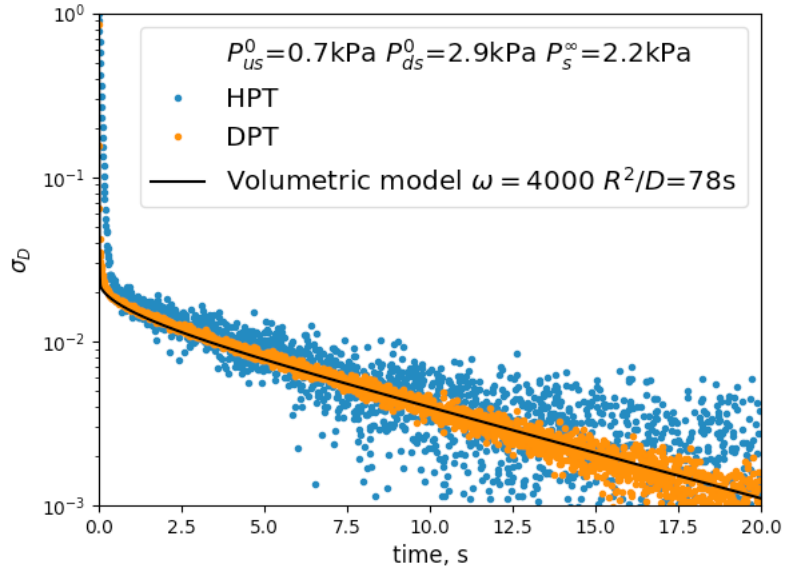

Fig. 7. Comparison of the reduced pressure response from HPT and DPT (N_2-4A pellet 35°C).

Fig. 7 shows the reduced pressure responses derived with the HPT and DPT signals using Eq. 6. The DPT curve exhibited better signal to noise ratio and allows to extract a more accurate diffusional time constant. The superiority of the DPT response was maintained at all the pressure levels.

Experiments at different pressures

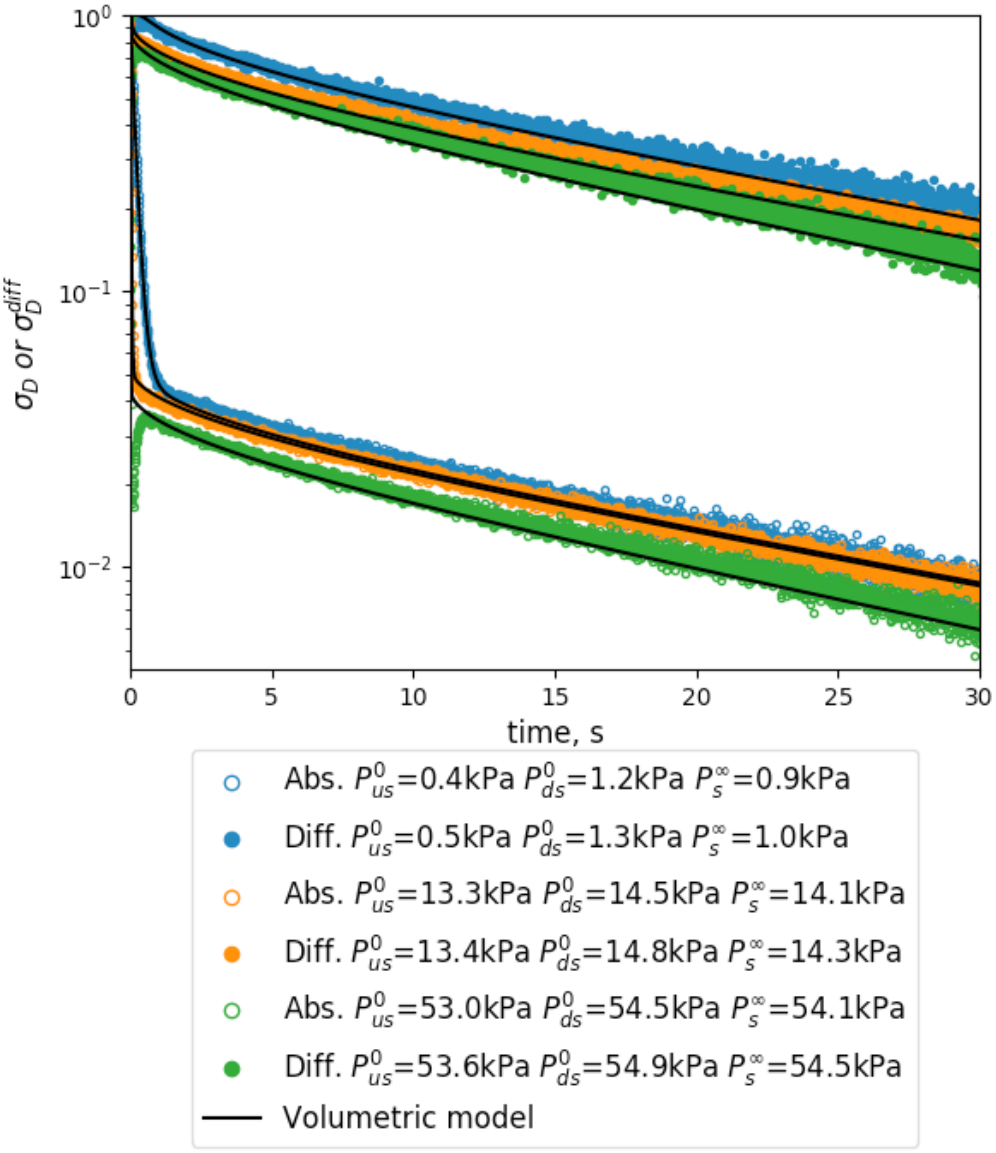

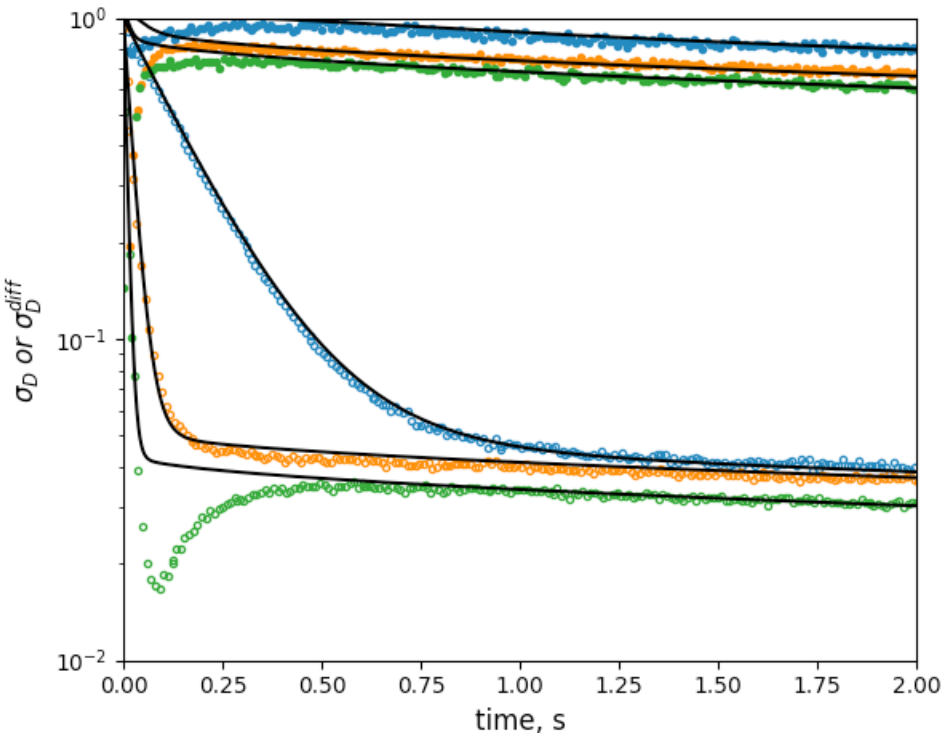

Fig. 8. Comparison of adsorption response curves of N_2 on a 4A pellet at different pressure levels (T = 5℃). Top: long time; bottom: short time. The diffusional time constant $\frac{R^2}{D} = 230s$ was used to match the curves at the two lower pressures (1 kPa and 14 kPa) and $\frac{R^2}{D} = 200s$ was used to match the 54 kPa curves.

Fig. 8 compares the reduced pressure response of N_2 adsorption on the 4A pellet at different pressures at the lowest experimental temperature of 5 ℃. Both absolute and differential mode curves are shown. The differential curves have higher intercept since the pressure drop due to the initial gas expansion is almost cancelled by the differential mode, as demonstrated in Eqs 6-8. For all the steps, the pressure changes in the sample cell ($P_S^{\infty} - P_{us}^0$) are smaller than 2 kPa. The small shift of intercept with increasing pressure is linked to the small decrease in the adsorption capacity and the dimensionless *K* values are 15, 13.5, 11.3 for the three pressures. There is no clear difference in the long-time slopes between the 1 kPa and 14 kPa curves and the time constant of 230s is used for both. The kinetics at 54 kPa were slightly faster and a time constant of 200s was obtained. This pattern of behaviour is consistent with the previous study by Ruthven and Derrah [50] in that the micropore diffusivity increases at higher concentration due to the nonlinearity of the isotherm. As the isotherm is more linear at 20℃ and 35℃, the diffusivity was found to be invariant with pressure and only a single time constant was extracted for each temperature.

It should also be noted that this set of data was obtained with the latest system configuration. To prevent sample contamination in the dosing volume, two 60 μm filters

were installed at the outlets of LV4 and LV5. The filter adds a resistance to the gas flow, thus resulting in a slower initial response especially at low pressures. This can be observed clearly in Fig. 8 (bottom) and the absolute mode response at 1kPa is directly affected by the filter up to ~1 s. The differential mode responses, by comparison, are almost not affected by the presence of the filters since their effects are largely cancelled by the double branch expansion. This shows the advantage of differential mode experiments over absolute mode experiments for fast diffusing systems. The slope that contains diffusion information appears ~0.8 s earlier than that of the absolute mode.

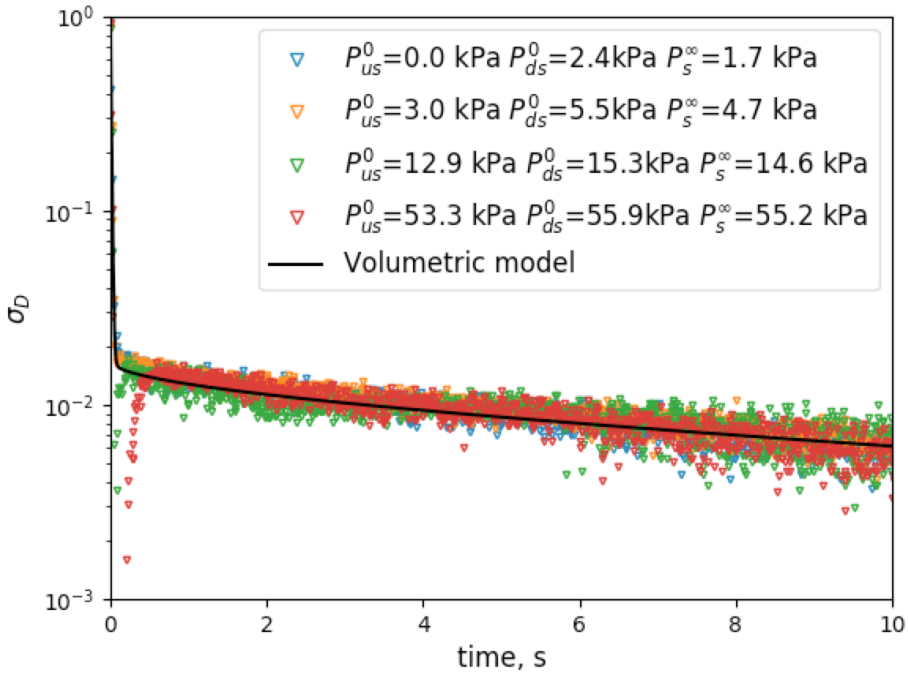

Fig. 9. Ar adsorption kinetics on 4A fragments at −10 ℃ and match with volumetric model: $\frac{R^2}{D} = 180s.$

Since Ar was more weakly adsorbed and there was a relatively higher uncertainty in the determined time constants at 35℃, additional experiments at a lower temperature –10℃ were performed to obtain a reliable activation energy. The kinetic curves of Ar on 4A fragments at −10 ℃ are shown in Fig. 9. Similarly to N_2, at each pressure adsorption and desorption experiments are performed and consistency of the two was checked. The intercept of the long-time asymptote of Ar was lower than N_2 due to the lower adsorbed amount. The fact that at the lowest experimental temperature all the curves at different pressures overlap indicates the linearity of the Ar-4A isotherm over the pressure range (0 – 55kPa) and this should also be true for higher experimental temperatures (5 – 35℃).

Summary of diffusional time constants at different temperatures

Since the fragment and pellet results show good agreement, the kinetic curves of the pellet are used to extract diffusional time constants due to the better signal to noise ratio. As the diffusivity is found to be almost constant over the pressure range studied, only the lowest pressure curves are presented here. The N_2 and Ar signals along with the volumetric model curves are shown in Fig. 10 and Fig. 11. With increasing temperature the intercept of the long-time asymptote was found to shift down due to the reduced adsorption capacity and the slope became steeper due to the increase in the diffusivity. Excellent match of long-time asymptotes with the isothermal volumetric model was obtained for both differential mode and absolute mode data.

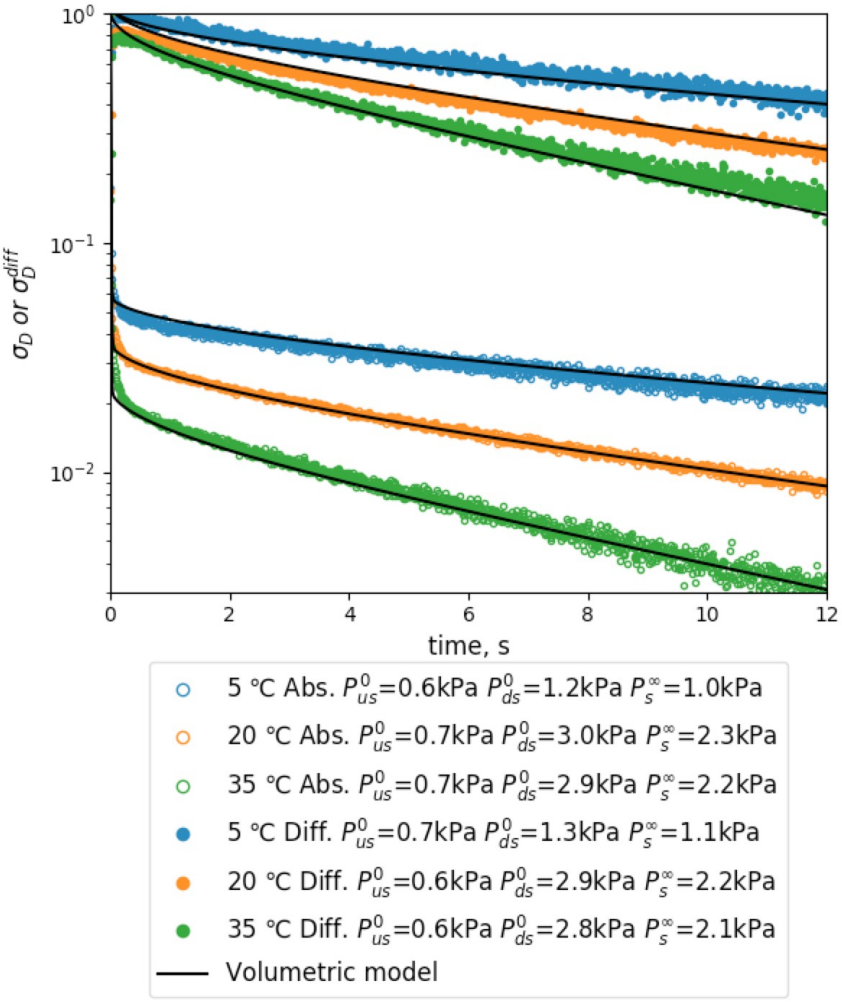

Fig. 10. Volumetric model match of N_2 kinetic response on 4A pellet. Model parameters are reported in Table 2.

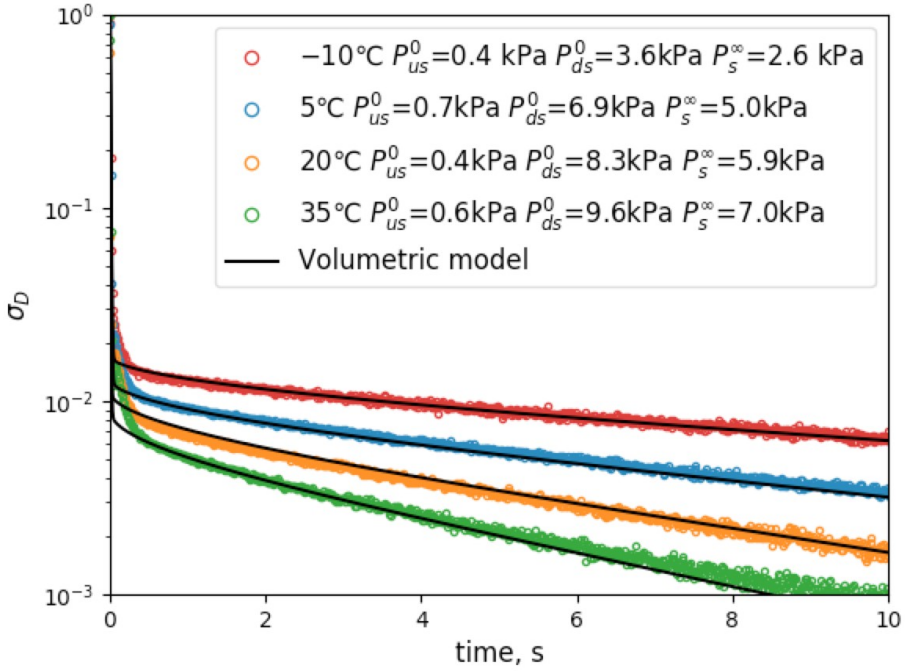

Fig. 11. Volumetric model match of Ar kinetic response on 4A pellet. Model parameters are reported in Table 2.

It can be noted from Fig. 11 that relatively large steps (~7kPa) are used for Ar at the higher temperatures. Due to the low adsorbed amount, these steps were found to be optimal for achieving a good signal while maintaining isotherm linearity and isothermal conditions. Generally there is a trade-off between these two conditions. A simple procedure to find the optimal step is to perform a small step experiment first and then increase the step gradually until the desired signal-to-noise ratio is obtained. In order to confirm the absence of any secondary effects, it is necessary to check that the long-time slope remains the same. A comparison of Ar signals with small and large steps is shown in the Supplementary Information.

Table 2 summarises the dimensionless slope of the isotherm, $K = \frac{R_g T_{us}(q_\infty - q_0)}{P_s^\infty - P_{us}^0}$, and the micropore diffusional time constants obtained. Both values decrease with temperature, corresponding to reduced adsorption capacity and an activated diffusion process. The absolute value of the slope of the isotherm is dependent on the value used for the solid volume as the experiment determines the adsorbed amounts directly, but this would not affect the diffusional time constants.

Table 2. Summary of dimensionless model parameters and diffusional time constants

	N_2					Ar				
T, ℃	δ	γ	ω	$\frac{R^2}{D}$, s	K	δ	γ	ω	$\frac{R^2}{D}$, s	K
–10	-	-	-	-	-	29.3	13.2	8000	180	4.4
5	8.3	3.6	10000	230	15.0	40.5	17.6	5000	108	3.4
20	14.2	6.0	5000	125	10.1	49.2	20.7	5000	70	2.9
35	23.9	9.8	4000	78	6.3	64.7	26.5	3000	50	2.3

Fig. 12 displays the Arrhenius plots for N_2 and Ar. For N_2 the values of D/R^2 at three temperatures conform well to the linear dependence vs 1/T while for Ar the value at 35 ℃ shows a slight deviation. This small deviation at the highest temperature is due to the uncertainty in the extracted time constant as a result of the small adsorbed amount. The D/R^2 values at the other three temperatures are deemed more reliable to determine the activation energy for Ar. The activation energies are listed in Table 3.

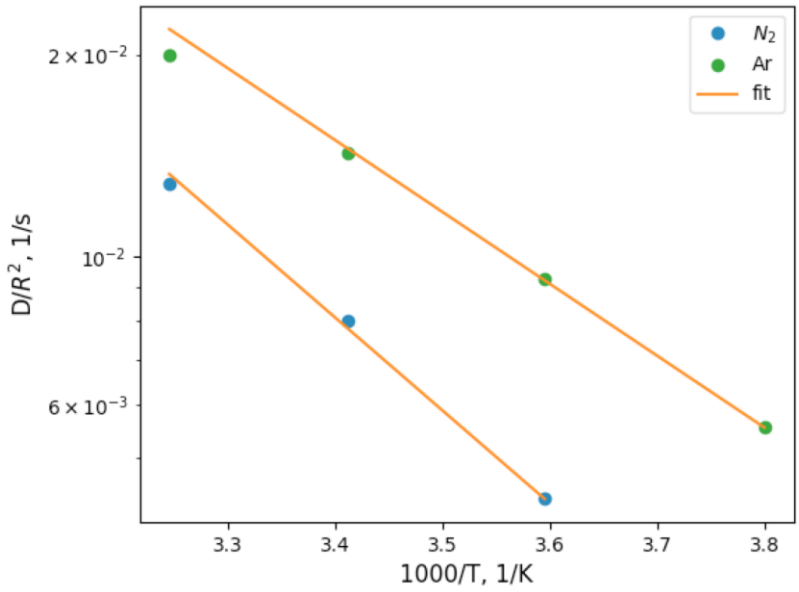

Fig. 12. Arrhenius plot of N_2 and Ar diffusion on zeolite 4A

Table 3. Comparison of activation energies with literature

	Technique	Sample	Crystal diameter, μm	Temperature range N_2, K	$E_{N_2}, kJ/mol$	Temperature range Ar, K	$E_{Ar}, kJ/mol$
Present study	Differential volumetric	UOP 4A pellet	1.85*	278-308	26.5	263-308	20.5
Cao et al. (2000) [51]	Tracer exchange	UOP 4A bead	1.95	253-333	21.9	-	-
Ruthven & Derrah (1975) [50]	Gravimetric	Linde 4A crystals	3.2	215-277	25.5	200-275	24.3
Van de Voorde et al. (1990) [52]	Chromatographic	Commercial 4A crystals	100-150	298-373	22	298-373	21
Shah & Oey (1988) [54]	Chromatographic	Linde 4A pellet	3.6	-	-	298-373	19.7
Eagan & Anderson (1975) [53]	Volumetric	Linde 4A crystals	4.1	195-213	34.7	173-193	19.7
Yucel & Ruthven (1980) [49]	Gravimetric	Linde 4A crystals	4.1	243-323	24.3	-	-

* Estimated with N_2 diffusivity from Cao et al. [51].

Table 3 also lists some previous studies on N_2 and Ar diffusion in commercial 4A pellets or crystals. It is evident that the activation energies obtained are in good agreement with those in the literature. Since the crystal size of the UOP sample is not known, the micropore diffusional time constant extracted cannot be directly converted to a diffusivity. However, if the N_2 diffusivity in a similar material measured by Cao et al. [51] is used to estimate the crystal size of the sample, a reasonable value of 1.85 μm is obtained.

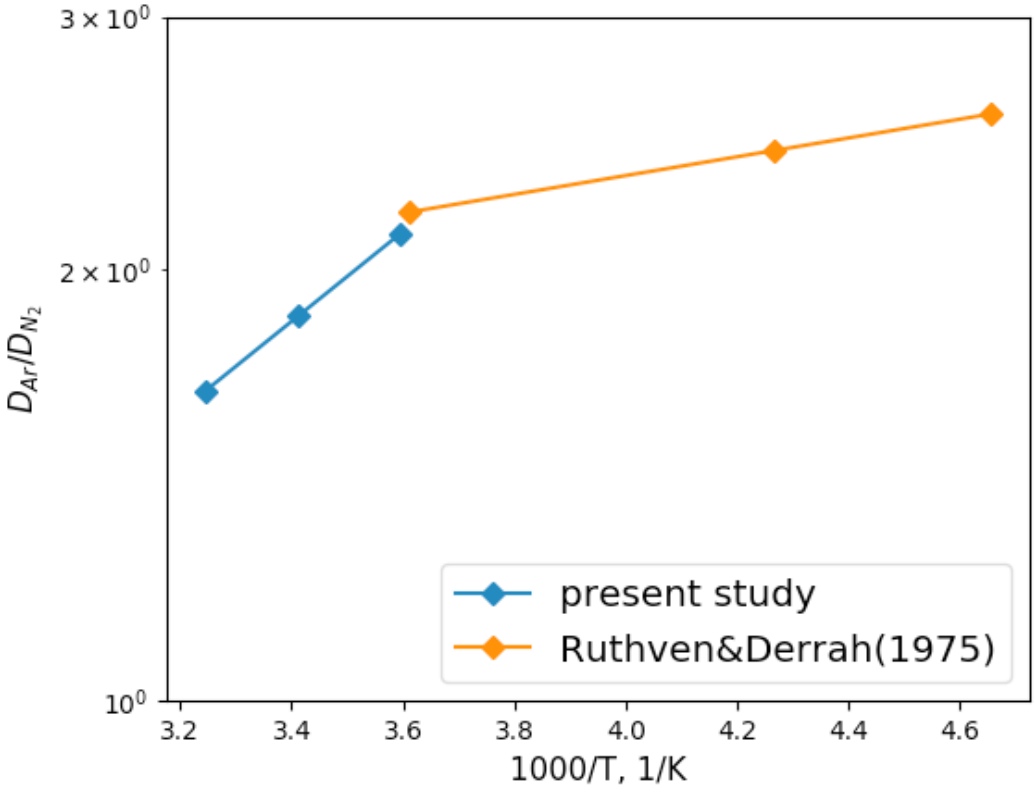

Fig. 13 Comparison of ratio of Ar diffusivity to N_2 diffusivity in zeolite 4A with Ruthven and Derrah [50].

To further validate our approach, the ratio of the Ar diffusivity to N_2 diffusivity is compared in Fig. 13 with the ratio from Ruthven and Derrah [50] who studied kinetics on 3.2μm crystals of Linde 4A zeolite using a gravimetric method. Although the diffusivity values can show large variations across different samples due to difference in the fraction of windows that are blocked by a cation or have undergone framework damage, these blockages should have the same effect on different molecules [63]. Therefore, the ratio D_{Ar}/D_{N_2} should not vary significantly between samples and it is also the parameter that determines the kinetic selectivity in a separation process [64]. The values shown in Fig. 13 are very close around 5℃, indicating good consistency. The main difference is due to the slightly lower activation energy for Ar found in the UOP pellet.

5. Conclusions

In this study, a novel differential volumetric apparatus (ADVA-1) developed for the accurate determination of gas diffusional time constants in nanoporous materials over the pressure range from vacuum to 130kPa was presented. On the ADVA-1 a $\pm$3.5 kPa differential pressure transducer was employed to measure adsorption kinetics and thanks to the fast data acquisition module, time constants of a few seconds can be measured. Since for kinetic

measurements a small sample mass is desirable to minimise any secondary effects, ADVA-1 was built with small cell volumes for high sensitivity and this allows the measurements of even weakly adsorbed molecules on individual beads or pellets.

To demonstrate the advantages of ADVA-1 and also to validate the system, N_2 and Ar diffusion in zeolite 4A fragments and a single pellet (both ~40 mg) were studied. The results showed that even for weakly adsorbed systems, a good signal-to-noise ratio can be achieved with a single pellet at all the experimental conditions. The consistency between fragment and pellet confirms that the measurements were isothermal and under micropore diffusion control, which is in line with literature data.

Both absolute and differential modes of the experiment have been demonstrated and yield consistent results. The approach has been validated in three aspects. Firstly, the activation energies, 26.5 kJ/mol for N_2 and 20.5 kJ/mol for Ar, are in good agreement with literature values. Secondly, with the N_2 diffusivity measured on a sample from the same manufacturer, the crystal size of the sample used in this study is estimated to be 1.85 μm, which is similar to values reported in the literature. Finally, the ratio between N_2 and Ar diffusivities is consistent with the ratio determined for 4A crystals by other researchers.

Acknowledgement

The financial support from Air Liquide for developing the ADVA-1 is gratefully acknowledged.

Notation

D	Micropore diffusivity, $m^2\ s^{-1}$
E	Activation energy, kJ mol^{-1}
K	Dimensionless slope of the isotherm, $\frac{R_g T_{us}(q_\infty - q_0)}{P_s^\infty - P_{us}^0}$
P	Absolute pressure, kPa
ΔP	Differential pressure, kPa
q	Adsorbed phase concentration, mol m^{-3}
R	Crystal radius, m

R_g	Ideal gas constant, J mol^{-1} K^{-1}
t	Time, s
Δt	Time lag between LV4 and LV5 opening for differential mode experiments, s
T_d	Temperature of dosing cell, K
T_u	Temperature of uptake cell, K
V_d	Volume of dosing cell, m^3
V_S	Volume of adsorbent solid, m^3
V_u	Volume of uptake cell, m^3

Superscript

0	Initial
∞	Final

Subscript

ds	Sample dosing
us	Sample uptake
dr	Reference dosing
ur	Reference uptake

Greek letters

β_i	Eigenvalues, Eq. 3
δ	1/3 ratio of accumulation in the dosing volume to accumulation in the solid
γ	1/3 ratio of accumulation in the uptake volume to accumulation in the solid

σ_D, σ_{ds}	Reduced pressure in dosing volume, Eq. 1; Reduced differential pressure under absolute mode, Eq. 6
σ_D^{diff}	Reduced differential pressure for differential mode experiments, Eq. 8
$\bar{\chi}$	Valve constant, $\mathrm{mol\ s^{-1}\ Pa^{-1}}$
ω	Ratio of diffusion time constant to the valve time constant
ω_r	Ratio of diffusion time constant to the valve time constant in reference branch

6. References

1. Brandani S., Brandani F., Mangano E., and Pullumbi P. Using a volumetric apparatus to identify and measure the mass transfer resistance in commercial adsorbents. *Microporous and Mesoporous Materials*. (2020) 304: 109277.

2. Wang J.-Y., Mangano E., Brandani S., and Ruthven D. M. A review of common practices in gravimetric and volumetric adsorption kinetic experiments. *Adsorption*. (2021) 27: 295–318.

3. Ruthven D. M., and Lee L. -K. Kinetics of nonisothermal sorption: Systems with bed diffusion control. *AIChE Journal*. (1981) 27: 654–663.

4. Ruthven D. M., Lee L.-K., and Yucel H. Kinetics of non-isothermal sorption in molecular sieve crystals. *AIChE Journal*. (1980) 26: 16–23.

5. Kočiřík M., Struve P., and Bülow M. Analytical solution of simultaneous mass and heat transfer in zeolite crystals under constant-volume/variable-pressure conditions. *Journal of the Chemical Society, Faraday Transactions 1*. (1984) 80: 2167–2174.

6. Kärger J., Ruthven D. M., and Theodorou D. N. *Diffusion in Nanoporous Materials*. (2012). Weinheim, Germany: Wiley-VCH Verlag GmbH & Co. KGaA.

7. Barrer R. M. Transient flow of gases in sorbents providing uniform capillary networks of molecular dimensions. *Transactions of the Faraday Society*. (1949) 45: 358–373.

8. Barrer R. M., and Brook D. W. Molecular diffusion in chabazite, mordenite and levynite. *Transactions of the Faraday Society*. (1953) 49: 1049–1059.

9. Riekert L. The kinetics of ethylene polymerization in nickel-Y zeolite. *Journal of Catalysis*. (1970) 19: 8–14.

10. Riekert L. Rates of sorption and diffusion of hydrocarbons in zeolites. *AIChE Journal*. (1971) 17: 446–454.

11. Koresh J., and Soffer A. Molecular sieve carbons. Part 3.—Adsorption kinetics according to a surface-barrier model. *Journal of the Chemical Society, Faraday Transactions 1: Physical Chemistry in Condensed Phases*. (1981) 77: 3005.

12. Voogd P., and Van Bekkum H. Diffusion of n-HEXANE and 3-Methylpentane in H-Zsm-5 Crystals of Various Sizes. *Studies in Surface Science and Catalysis*. (1989) 46: 519–531.

13. Voogd P., and van Bekkum H. The Adsorptive and Reaction Limiting Diffusion of 2,3-Dimethylbutane in Large Crystals of (Aluminated) Silicalite-1. *Industrial and Engineering Chemistry Research*. (1991) 30: 2123–2133.

14. Loughlin K. F., Hassan M. M., Fatehi A. I., and Zahur M. Rate and equilibrium sorption parameters for nitrogen and methane on carbon molecular sieve. *Gas Separation and Purification*. (1993) 7: 264–273.

15. Hu Z., and Vansant E. F. Carbon molecular sieves produced from walnut shell. *Carbon*. (1995) 33: 561–567.

16. Hernández-Huesca R., Díaz L., and Aguilar-Armenta G. Adsorption equilibria and kinetics of CO_2, CH_4 and N_2 in natural zeolites. *Separation and Purification Technology*. (1999) 15: 163–173.

17. Bülow M., Struve P., Finger G., Redszus C., Ehrhardt K., Schirmer W., and Kärger J. Sorption kinetics of n-hexane on MgA zeolites of different crystal sizes: Study of the rate-limiting transport mechanism. *Journal of the Chemical Society, Faraday Transactions 1: Physical Chemistry in Condensed Phases*. (1980) 76: 597–615.

18. Bülow M., Struve P., and Pikus S. Influence of hydrothermal pretreatment on zeolitic diffusivity detected by comparative sorption kinetics and small-angle X-ray scattering investigations. *Zeolites*. (1982) 2: 267–270.

19. Bülow M., Mietk W., Struve P., and Lorenz P. Intracrystalline diffusion of benzene in NaX zeolite studied by sorption kinetics. *Journal of the Chemical Society, Faraday Transactions 1: Physical Chemistry in Condensed Phases*. (1983) 79: 2457–2466.

20. Bülow M., Lorenz P., Mietk W., Struve P., and Samulevič N. N. Sorption kinetics of neopentane on NaX zeolites of different crystal sizes. *Journal of the Chemical Society, Faraday Transactions 1: Physical Chemistry in Condensed Phases*. (1983) 79: 1099–1108.

21. Bülow M., Struve P., Mietk W., and Kočiřik M. Experimental evidence of the influence of sorption-heat release processes on the sorption kinetics of benzene in NaX zeolite crystals. *Journal of the Chemical Society, Faraday Transactions 1: Physical Chemistry in Condensed Phases*. (1984) 80: 813–822.

22. Zikánová A., Bülow M., and Schlodder H. Intracrystalline diffusion of benzene in ZSM-5 and silicalite. *Zeolites*. (1987) 7: 115–118.

23. Kärger J., Pfeifer H., Stallmach F., Bülow M., Struve P., Entner R., Spindler H., and Seidel R. Influence of molecular shape on probing mass transfer resistances on zeolites. *AIChE Journal*. (1990) 36: 1500–1504.

24. Micke A., and Bülow M. Sorption kinetics of benzene on a gallosilicate with MFI structure. *Microporous Materials*. (1994) 3: 185–193.

25. Micke A., Bülow M., and Kočiřík M. A nonequilibrium surface barrier for sorption kinetics of p-ethyltoluene on ZSM-5 molecular sieves. *Journal of Physical Chemistry*. (1994) 98: 924–929.

26. Bülow M. Letter to the editor. *Adsorption*. (2021) 20: 135–136.

27. Hashimoto K., Masuda T., and Kawase M. Measurement of Intracrystalline Diffusivities of Hzsm-5 Zeolite At Higher Temperatures and Predictions of Shape Selectivity. In *Studies in Surface Science and Catalysis*. (1989) (Vol. 46, pp. 485–494).

28. Hashimoto K., Masuda T., and Murakami N. Intracrystalline Diffusivities of Hzsm-5 Zeolites. In *Studies in Surface Science and Catalysis*. (1991) (Vol. 69, pp. 477–484).

29. Masuda T., Murakami N., and Hashimoto K. Intracrystalline diffusivities of coked HZSM-5 zeolite. *Chemical Engineering Science*. (1992) 47: 2775–2780.

30. Masuda T., and Hashimoto K. Measurements of Adsorption on Outer Surface of Zeolite and their Influence on Evaluation of Intracrystalline Diffusivity. In *Studies in Surface Science and Catalysis*. (1994) (Vol. 83, pp. 225–232).

31. Masuda T., Fukada K., Fujikata Y., Ikeda H., and Hashimoto K. Measurement and prediction of the diffusivity of Y-type zeolite. *Chemical Engineering Science*. (1996) 51: 1879–1888.

32. Masuda T., Fujikata Y., Nishida T., and Hashimoto K. The influence of acid sites on intracrystalline diffusivities within MFI-type zeolites. *Microporous and Mesoporous Materials*. (1998) 23: 157–167.

33. Fujikata Y., Masuda T., Ikeda H., and Hashimoto K. Measurement of the diffusivities within MFI- and Y-type zeolite catalysts in adsorption and desorption processes. *Microporous and Mesoporous Materials*. (1998) 21: 679–686.

34. Ackerman W. C., Hua D. W., Kim Y. W., Huling J. C., and Smith D. M. Adsorption Studies Of Pure And Modified Imogolite As A Potential Pore Size Standard. *Studies in Surface Science and Catalysis*. (1994) 87: 735–744.

35. Rege S. U., Padin J., and Yang R. T. Olefin/Paraffin Separations by Adsorption: π-Complexation vs. Kinetic Separation. *AIChE Journal*. (1998) 44: 799–809.

36. Huang Q., Sundaram S. M., and Farooq S. Revisiting transport of gases in the micropores of carbon molecular sieves. *Langmuir*. (2003) 19: 393–405.

37. Qinglin H., Farooq S., and Karimi I. A. Binary and Ternary Adsorption Kinetics of Gases in Carbon Molecular Sieves. *Langmuir*. (2003) 19: 5722–5734.

38. Marathe R. P., Mantri K., Srinivasan M. P., and Farooq S. Effect of ion exchange and dehydration temperature on the adsorption and diffusion of gases in ETS-4. *Industrial and Engineering Chemistry Research*. (2004) 43: 5281–5290.

39. Marathe R. P., Farooq S., and Srinivasan M. P. Modeling Gas Adsorption and Transport in Small-Pore Titanium Silicates. *Langmuir*. (2005) 21: 4532–4546.

40. Brandani S., Mangano E., Brandani F., and Pullumbi P. Carbon dioxide mass transport in commercial carbon molecular sieves using a volumetric apparatus. *Separation and Purification Technology*. (2020) 245: 116862.

41. Rouquerol J., and Rouquerol F. Methodology of Gas Adsorption. In *Adsorption by Powders and Porous Solids: Principles, Methodology and Applications: Second Edition*. (2013) (pp. 57–104).

42. Zielinski J. M., Coe C. G., Nickel R. J., Romeo A. M., Cooper A. C., and Pez G. P. High pressure sorption isotherms via differential pressure measurements. *Adsorption*. (2007) 13: 1–7.

43. Browning D. J., Gerrard M. L., Lakeman J. B., Mellor I. M., Mortimer R. J., and Turpin M. C. Studies into the Storage of Hydrogen in Carbon Nanofibers: Proposal of a Possible Reaction Mechanism. *Nano Letters*. (2002) 2: 201–205.

44. Qajar A., Peer M., Rajagopalan R., and Foley H. C. High pressure hydrogen adsorption apparatus: Design and error analysis. *International Journal of Hydrogen Energy*. (2012) 37: 9123–9136.

45. Blackman J. M., Patrick J. W., and Snape C. E. An accurate volumetric differential pressure method for the determination of hydrogen storage capacity at high pressures in carbon materials. *Carbon*. (2006) 44: 918–927.

46. Haq N., and Ruthven D. M. Chromatographic study of sorption and diffusion in 4A zeolite. *Journal of Colloid and Interface Science*. (1986) 112: 154–163.

47. SARMA N., and HAYNES H. W. APPLICATION OF GAS-CHROMATOGRAPHY TO MEASUREMENTS OF DIFFUSION IN ZEOLITES. *ADVANCES IN CHEMISTRY SERIES*. (1974) 205–217.

48. Shah D. B., and Ruthven D. M. Measurement of zeolitic diffusivities and equilibrium isotherms by chromatography. *AIChE Journal*. (1977) 23: 804–809.

49. Yucel H., and Ruthven D. M. Diffusion in 4A zeolite. Study of the effect of crystal size. *Journal of the Chemical Society, Faraday Transactions 1: Physical Chemistry in Condensed Phases*. (1980) 76: 60.

50. Ruthven D. M., and Derrah R. I. Diffusion of monatomic and diatomic gases in 4A and 5A zeolites. *Journal of the Chemical Society, Faraday Transactions 1: Physical Chemistry in Condensed Phases*. (1975) 71: 2031–2044.

51. Cao D. V., Mohr R. J., Rao M. B., and Sircar S. Self-diffusivities of N_2, CH_4, and Kr on 4A zeolite pellets by isotope exchange technique. *Journal of Physical Chemistry B*. (2000) 104: 10498–10501.

52. Van de Voorde M., Tavernier Y., Martens J., Verelst H., Jacobs P., and Baron G. V. Chromatographic Study of Adsorption Equilibria and Micropore Diffusion Constants of Permanent Gases in Synthetic Zeolites of the LTA, FAU and SOD Type. (1990). Elsevier Sci. Publ. BV; Amsterdam.

53. Eagan J. D., and Anderson R. B. Kinetics and equilibrium of adsorption on 4A zeolite. *Journal of Colloid and Interface Science*. (1975) 50: 419–433.

54. Shah D. B., and Oey N. K. Application of method of moments to highly skewed responses. *Zeolites*. (1988) 8: 404–408.

55. Brandani S. Analysis of the piezometric method for the study of diffusion in

microporous solids: Isothermal case. *Adsorption*. (1998) 4: 17–24.

56. Bae Y.-S., and Lee C.-H. Sorption kinetics of eight gases on a carbon molecular sieve at elevated pressure. *Carbon*. (2005) 43: 95–107.

57. Long C., and Guan J. Measurement of Diffusivity and Thermal Parameters of Gas Adsorption with a Volumetric Method. *Industrial & Engineering Chemistry Research*. (2012) 51: 6502–6512.

58. Wang Y., and Liu S. Estimation of Pressure-Dependent Diffusive Permeability of Coal Using Methane Diffusion Coefficient: Laboratory Measurements and Modeling. *Energy & Fuels*. (2016) 30: 8968–8976.

59. Du X., Gu M., Hou Z., Liu Z., and Wu T. Experimental Study on the Kinetics of Adsorption of CO_2 and CH_4 in Gas-Bearing Shale Reservoirs. *Energy & Fuels*. (2019) 33: 12587–12600.

60. Abedini H., Shariati A., and Khosravi-Nikou M. R. Adsorption of propane and propylene on M-MOF-74 (M=Cu, Co): Equilibrium and kinetic study. *Chemical Engineering Research and Design*. (2020) 153: 96–106.

61. Maghsoudi H., Abdi H., and Aidani A. Temperature- and Pressure-Dependent Adsorption Equilibria and Diffusivities of Propylene and Propane in Pure-Silica Si-CHA Zeolite. *Industrial & Engineering Chemistry Research*. (2020) 59: 1682–1692.

62. Kang Y., Huang F., You L., Li X., and Gao B. Impact of fracturing fluid on multi-scale mass transport in coalbed methane reservoirs. *International Journal of Coal Geology*. (2016) 154–155: 123–135.

63. Ruthven D. M. Diffusion in type A zeolites: New insights from old data. *Microporous and Mesoporous Materials*. (2012) 162: 69–79.

64. Luberti M., and Ahn H. Design of an industrial multi-bed (V)PSA unit for argon concentration. *Separation and Purification Technology*. (2021) 261: 118254.

Supplementary Information

A Novel Adsorption Differential Volumetric Apparatus to Measure Mass Transfer in Nanoporous Materials

Jin-Yu Wang[a], Enzo Mangano[a], Stefano Brandani[a*], Federico Brandani[b] and Pluton Pullumbi[b]

[a] School of Engineering, The University of Edinburgh, King's Buildings, Edinburgh, EH9 3FB, UK

[b] Campus Innovation Paris, Air Liquide, Paris, France

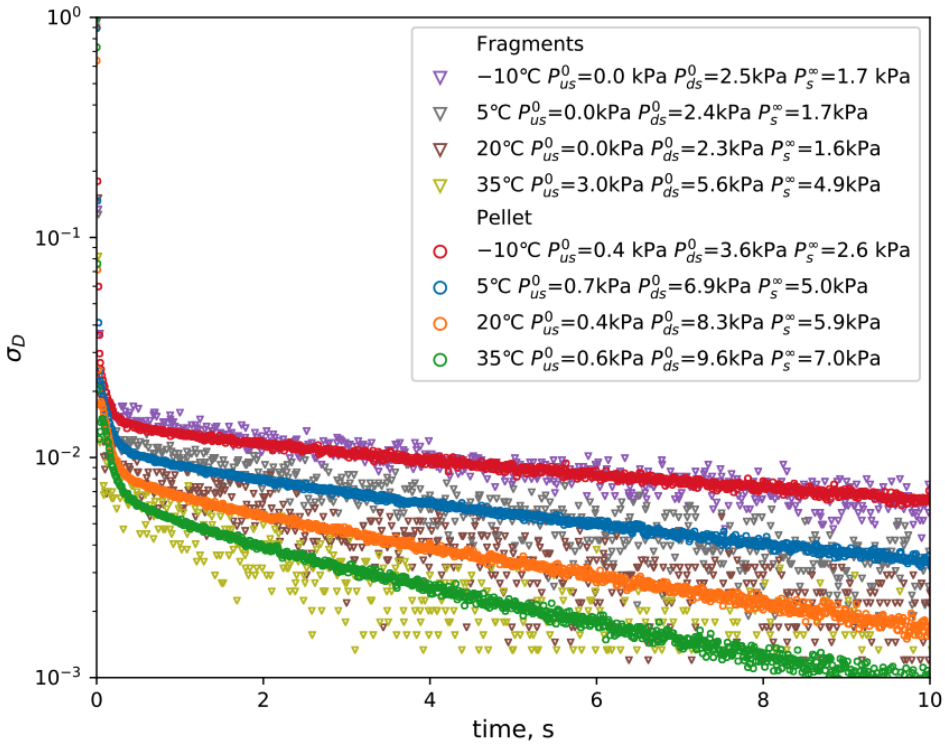

Fig. S1. Comparison of Ar adsorption kinetics on 4A fragments and pellet at 4 temperatures. The fragment signals are plotted at reduced frequency (50 Hz) for better visibility.

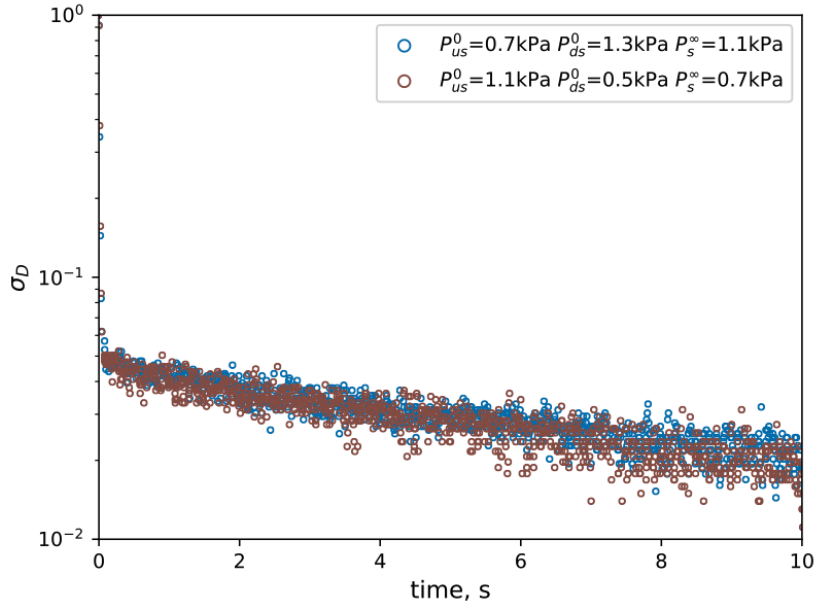

Fig. S2. Comparison of adsorption and desorption reduced pressure responses for N_2 –4A fragments at 1 kPa (5℃).

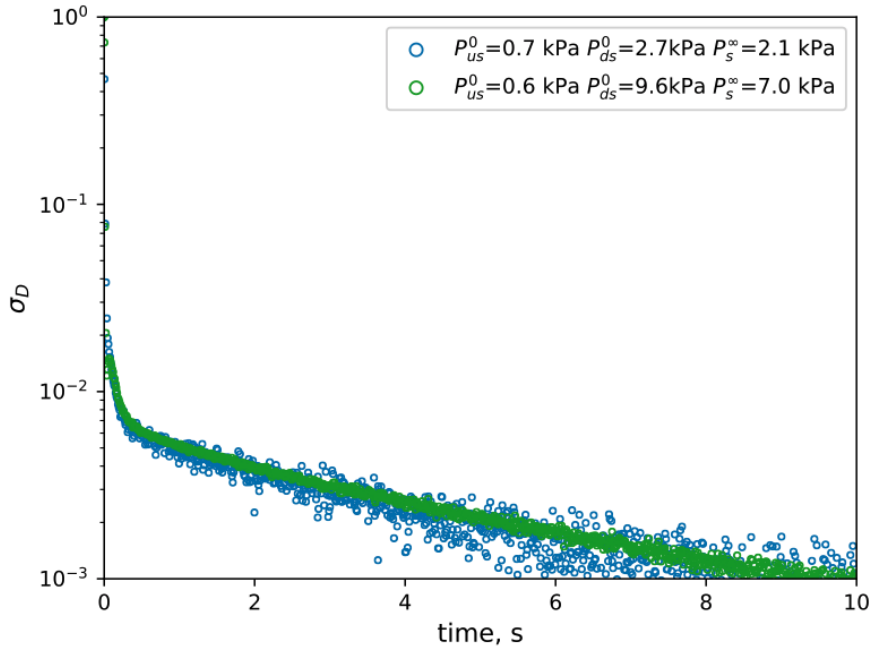

Fig. S3. Comparison of two pressure steps for Ar adsorption on 4A single pellet at 35℃.